



A free time point model for dynamic contrast enhanced exploration

Levebvre Julie, Djebali Ikram, Perez-Liva Mailyn, Lecler Augustin,
Bouchouicha Afef, Sourdon Joevin, Isma Bentoumi, Charles-André Cuenod,
Balvay Daniel

► To cite this version:

Levebvre Julie, Djebali Ikram, Perez-Liva Mailyn, Lecler Augustin, Bouchouicha Afef, et al.. A free time point model for dynamic contrast enhanced exploration. *Magnetic Resonance Imaging*, 2021, 80, pp.39-49. 10.1016/j.mri.2021.04.005 . hal-03545879

HAL Id: hal-03545879

<https://hal.science/hal-03545879v1>

Submitted on 9 May 2023

HAL is a multi-disciplinary open access archive for the deposit and dissemination of scientific research documents, whether they are published or not. The documents may come from teaching and research institutions in France or abroad, or from public or private research centers.

L'archive ouverte pluridisciplinaire **HAL**, est destinée au dépôt et à la diffusion de documents scientifiques de niveau recherche, publiés ou non, émanant des établissements d'enseignement et de recherche français ou étrangers, des laboratoires publics ou privés.



Distributed under a Creative Commons Attribution - NonCommercial 4.0 International License

A free time point model for Dynamic Contrast Enhanced exploration.

Levebvre Julie (MS)^A, Djebali Ikram (MS)^A, Perez-Liva Mailyn (PhD)^A, Lecler Augustin (PhD, MD)^A,
Bouchouicha Afef (PhD)^A, Sourdon Joevin (PhD)^A, Isma Bentoumi^A, Charles-André Cuenod (PhD, MD)^{A,B},
Balvay Daniel (PhD)^{A,C}

^A Université de Paris, PARCC, INSERM, F-75015 Paris, France.

^B Service Radiologie, AP-HP, Hôpital Européen Georges Pompidou, F-75015, France

^C Université de Paris, Plateforme d'Imageries du Vivant, F-75015, France

Research Article: 5940 words

Keywords: Convolution, Dynamic Systems Modeling for Prediction, Reliability, Signal synthesis

Levebvre Julie: julielefebvre.pro27@gmail.com

Ikram Jebali: djebali.ikram@gmail.com

Mailyn Perez Liva: mailyn.perez-liva@inserm.fr

Augustin Lecler : alecler@for.paris

Afef Bouchouicha : afef.bouchouicha@gmail.com

Joevin Sourdon: joevin.sourdon@univ-amu.fr

Isma Bentoumi: ibentoumi@hotmail.fr

Charles-André Cuénod: charles-andre.cuenod@aphp.fr

Corresponding author: daniel.balvay@inserm.fr

Daniel Balvay, PARCC-HEGP (Eq2)

56 rue Leblanc, 75015 PARIS, FRANCE

Tel: +33 1 53 98 8038

Fax: +33 1 53 98 79 52

Declarations of interest: none

1 INTRODUCTION

Dynamic-Contrast-Enhanced (DCE) imaging has shown great potential for diagnosis and prediction of patient's response to treatments [1–7]. As DCE data depend on the microcirculation characteristics of the tissue, it is a suitable technique to detect microcirculation disorders associated with pathologies such as tumors or ischemia. Under reproducible acquisition conditions and the same model for data analysis, the identification of patterns in DCE data can help classifying patients into different physiopathological groups [8–10].

Numerous studies pointed to the improvement of diagnosis and prognosis provided by DCE-MRI. As DCE has been mainly used for patient classification, simple analysis models have been favored as they are efficient to answer this question [11]. The simplicity and stability of these models are necessary to establish reliable and repeatable diagnostics [12,13]. Unfortunately, this use has led to little feedbacks in terms of pharmacokinetic (PK) or molecular interpretation. However, many published and commercially available PK models provide interpretive and quantitative parameters related with microcirculatory tissue characteristics, such as “blood flow” or “interstitial volume” [14]. The interpretation of such models is generally justified by reasonable qualitative assumptions, *but these are only declarative interpretations that vary according to the models, which leads to a great variability of quantitative results depending on the model used* [15–18]. To verify interpretation, we must *at least* ensure that the assumptions are not contradicted by the observations. *It is therefore necessary to verify that the pharmacokinetic model correctly describes the DCE data before interpreting its parameters physiologically.* However, this is not generally done, as classification takes priority. Thus, models that were well-designed to classify patients are not automatically relevant for physiological interpretation [17] and then care must be taken in the physiological interpretation of DCE models.

However, for DCE users, there is a latent necessity for DCE users for new and trustable insights in terms of physiopathological interpretation [19–21]. Several studies have proposed techniques to compare the relevance of PK models with respect to the DCE data [22–26]. *But, so far, and in accordance with classification, these evaluations are more concerned with technical performance [27] than with data agreement.* The evaluation of this agreement is not trivial in DCE, explaining why it is generally not evaluated. To the best of our knowledge, the main obstacle is that PK models cannot be compared *directly* with DCE data. Indeed, the PK models do not describe the DCE data themselves but a transition between an arterial input and a tissue measurement. *In this work, our hypothesis is that a model specifically designed to have good agreement with the DCE data, under a wide range of experimental conditions, could act as an intermediate to assess the agreement of PK models versus DCE data.* Indeed, if such a reference model exists, it can describe the DCE data accurately and without bias. The agreement between a PK model and the DCE data, not directly measurable, can then be assessed by measuring the agreement between the PK model and the reference model. The first question is then to know if such a reference model is technically viable. We, therefore, sought to propose and test a model on several simulated data.

DCE data are highly variable due to the diversity of acquisition conditions [28], organs and pathologies studied. To correctly describe DCE data beyond simple targeted cases, we considered a model with minimal hypotheses. This, therefore, precludes using the parametric PK models currently available in the literature. Nevertheless, raw non-parametric models are known to be particularly unstable [29]. To improve its stability, non-parametric models are usually combined with appropriate regularization rules. A pioneering model with minimal hypotheses was proposed by Jerosch-Herold for cardiac applications [29]. It uses time decimation, to reduce the model dimension, followed by a B-Splines reconstruction. It was derived from deconvolution techniques [30]. However, this model presents casual oscillations that are not compatible with the latent physiology of the organ. In this work, we aimed to extend and optimize this model to build a potential reference model. It resulted in the Free-Time-Point

Hermite (FTPH) model, which was tested and compared against the original B-Spline.

We evaluated the FTPH model using simulations to investigate its ability to describe properly tissue information available in several types of DCE data. For this purpose, we generated data with the contrasting Two-Compartment exchange (2CX) and the Adiabatic Tissue Homogeneity (ATH) models described below [31], and checked numerically whether our model could fit both types of data accurately.

We then assessed whether the description of the data provided by the FTPH model was of sufficiently high quality to allow both experienced and inexperienced users to identify the models used to generate the data. The question then was whether the FTPH model allowed the user to find the physiological hypothesis in agreement with his data. Relying on the FTPH results, users were asked to estimate the most likely pharmacokinetic hypothesis to explain the data (2CX or ATH). The predictive value of this observation was then quantified. Finally, several real datasets were fitted with the FTPH model to assess the model response against real explorations.

2 MATERIAL AND METHODS

2.1 Convolutional Models

Most pharmacokinetic models found in literature, for MRI, CT and PET, assume that the measured Tissue Response (TIC(t)) results from a linear and invariant process over time derived from the arterial input function (AIF) signal. AIF corresponds to the contrast agent (CA) concentration coming from the arteries to be delivered into tissue. This leads to the following theoretical relationship between CA concentration in the AIF(t) and the CA concentration in the tissue TIC(t) for successive time points t:

$$TIC(t) = \int_0^t AIF(t - \tau) \cdot TIR(\tau) d\tau = AIF * TIR \quad (1)$$

where TIC(t) results from a convolution (*) of AIF(t) with a tissue impulse response TIR(t). The TIR signal corresponds with the amount of contrast agent remaining in the tissue after a unique input of CA at the initial time point. By definition, the TIR should be a positive and decreasing function.

2.2 Deconvolution techniques

2.2.1 Singular Value Decomposition

Deconvolution techniques consist of extracting the TIR(t) curve from AIF and TIC. Estimating TIR(t) is ideally equivalent to remove the influence of the AIF from TIC. It produces a signal that is less dependent on the experimental conditions. Estimating the set of parameters {p} of a pharmacokinetic model involves estimating the parametric impulse response corresponding to the model: TIR(t, {p}). Thus, some authors equate parametric estimation with deconvolution. In this paper, a minimal-hypothesis model was used, meaning a model describing only TIR values, with no assumptions other than its expected decrease.

Common deconvolution techniques use a matrix formalism to evaluate TIR for data defined by iterative measures. To simplify, AIF(t) and TIR(t) could be considered constant over short time intervals. Therefore, (1) can be reformulated with the following numerical approximation:

$$TIC(t_i) = TIC_i = \sum_{j=1}^i AIF(t_i - \tau_j) \cdot TIR(\tau_j) \cdot \Delta t + \epsilon_i = \sum_{j=1}^i A_{i,j} \cdot TIR + \epsilon_i \quad (2)$$

where Δt is the sampling interval and ε_i the noise in the signal. This approximation should be refined, without changes in formalism, by preliminary filtering the *AIF* signal for noise reduction and by oversampling data with any interpolation technique.

Equation (2) could be written with a matrix product:

$$TIC = \mathbf{A} \cdot TIR + \varepsilon \quad (3)$$

where *TIC*, *TIR* and ε are time signals and the matrix \mathbf{A} is defined as follows:

$$\mathbf{A} = \begin{bmatrix} AIF_1 & 0 & \dots & 0 \\ AIF_2 & AIF_1 & \dots & 0 \\ \vdots & \vdots & \ddots & \vdots \\ AIF_N & AIF_{N-1} & \dots & AIF_1 \end{bmatrix} \cdot \Delta t, \quad \mathbf{A} \in \mathbf{R}^{N \times N} \quad (4)$$

being N is the number of time points.

The direct inversion (3) to determine the impulse response from \mathbf{A} and *TIC* leads to an ill-posed problem and small perturbation in the measured data can cause deleterious instabilities in the *TIR* assessment. Several regularization techniques have been proposed, mainly by truncating the singular values that produce the strongest noise amplifications and by including regularization terms in the inversion [32–34]. A pseudo-inverse method with singular value decomposition (SVD) and Tikhonov regularization was used to solve (3) by limiting noise amplification. This method consists of diagonalizing the matrix \mathbf{A} enabling a pseudo inversion of \mathbf{A} to obtain *TIR* in (3). Each resulting diagonal element of matrix \mathbf{A} , named «singular value» corresponds to an amplification factor for specific time vectors. We used the freely available Matlab toolbox proposed by Hansen [32] to perform this decomposition.

B-spline approximation (see Fig. 1a)

Since regularized deconvolution techniques do not always provide stable DCE estimates, Jerosch-Herold proposed to reduce the deleterious high dimension of the problem by a B-Spline representation of the *TIR* signal [35]. This model represents *TIR* as a sum of weighted B-spline polynomial functions of degree n :

$$TIR(t_i) = \sum_{j=1}^p \alpha_j \cdot B_j^n(t_i) \quad , \alpha_j \in \mathbf{R}. \quad (5)$$

Here $B_j^n(t_i)$ represents the j^{th} basis spline function of degree n , and α_j is the corresponding B-spline coefficient. The set of t_i corresponds to the list of control points of the B-Spline approximation. A spline polynomial of degree n is a piecewise curve that has specific continuity properties: the curve is differentiable up to $n-1$ and is defined by a list of $p+n+1$ knots [30]. Roughly, this down-sampling technique reduces the $\mathbf{N} \times \mathbf{N}$ matrix \mathbf{A} by a $\mathbf{N} \times \mathbf{p}$ matrix \mathbf{D} as described in the following equation. (See [30,35] for a more detailed description).

$$TIR(t_i) = \sum_{j=1}^N \alpha_j \int_0^{t_i} B_j^n(s) \cdot AIF(t_i - s) ds = \sum_{j=1}^p \mathbf{D}_{i,j} \cdot \alpha_j \quad (6)$$

The estimation of *TIR* results, then from the evaluation of the vector α , by using the SVD technique including the Tikhonov regularization as described previously. The procedure thus consists of reducing the size of the model from N to p using regular sampling of the data, then reconstructing a regularized curve at N points using B-splines. We used the B-Spline model as a reference to compare with our model. The number of control points (p) was fixed to 15 and the 4th degree of B-Spline as proposed in the original publication.

2.2.2 Free Time Point Hermite model (see Fig. 1b)

The initial down-sampling of the control points of the *TIR* curve results from low-pass filtering of the estimated *TIR* by a frequency cutoff. However, in common parametric models, *TIR*s are generally characterized by sharp patterns at the beginning of the curve corresponding to fast flows into the vascular spaces, and smoother patterns at the end of the curve corresponding to slower flows out of the vascular spaces. Associating a single maximum frequency to the whole curve is therefore not necessarily appropriate and could cause an under-sampling of the initial part (bias of the estimated *TIR* curve), combined with an over-sampling of its final part (noise). To describe local sharp signal with a moderate cost in terms of model dimension (robustness), the homogeneous time points of the initial Jerosh-Herorl model were replaced by flexible time points in our model. The associated times of the different control points then become parameters to be estimated.

Moreover, the formalism of the B-Spline is complex and implicit, with no direct correspondence between the B-Spline parameters and the detailed properties of the *TIR* curve. This complicates the imposition of the decay constraint. Thus, the B-Spline formalism was replaced by a more direct spline interpolation formalism, where *TIR* signals were defined by few reference points included in the *TIR* curve. Hence, the *TIR* curve was described by some of its points (the reference points) which were defined each by an abscissa and an ordinate. The decrease of *TIR* was performed by imposing a decrease intensity of the successive reference point: $TIR(\tau_i)$. More precisely, values were evaluated iteratively as $TIR(\tau_i) = \beta_i \cdot TIR(\tau_{i-1})$ for any $i > 1$, where the attenuation factor β_i was defined between 0 and 1. Additionally, 3 null points were used to create a discontinuity before τ_1 and ensures zero *TIR* values before this time point.

Finally, Splines were used to interpolate *TIR* points between reference points. However, conventional Splines are known to generate oscillation between reference-point, and thus could contradict the decreasing hypothesis. To propagate the decrease between the reference points, the conventional splines were replaced by the specific cubic Hermite splines, consisting of a piecewise cubic C^1 splines [30]. Hermite interpolation conditions are often referred to as Piecewise Cubic Hermite Interpolating Polynomials (PCHIP). Due to the C^1 property of Hermite polynomial, the monotony of the curve is conserved between reference points.

Six reference-points defined with abscissa and ordinate, were used with the Free Time Point Hermite (FTPH) model for a reasonable comparison with the 15 parameters used to describe the ordinates of the initial B-Splines model. An iterative nonlinear least square fitting technique, as is currently used for parametric models, was used to fit the data with the FTPH model. In practice, curve-fitting was solved with the “lsqcurvefit” function of MATLAB R2013b (Matworks, Natick, MA) based on a “Trust-Region-Reflective Optimization” [36].

Both the control-points of B-splines and the reference-points for interpolating splines will be considered uniformly as “construction-points” throughout the rest of the paper.

2.3 Evaluation of the FTPH model (Fig. 2)

2.3.1 Data generation

The evaluation of the model accuracy, its robustness and its neutrality to data type were tested with simulated data. An AIF was selected randomly from a previous DCE-MRI clinical study [37] with principal investigators’ authorization. The main parameters of the MR sequence used are available in Table 1. Two different parametric models [14,31] were used to generate tissue enhancements. They were selected to represent data resulting from two contrasting assumptions on CA distribution in the vascular space of the tissue of interest. The 2CX model (model 1) assumes an instantaneous CA dilution in the vascular space. This principle induces an exponentially decreasing function for the vascular contribution in the *TIR*. The ATH model (model 2) assumes a null CA dilution in the vascular space, also considered as a set of homogeneous tubes. In this model, all the CA in the vascular space comes out at a given time, meaning that no CA comes out before (*TIR* presenting an initial plateau) and that no CA remains in the vascular space after. Both models include an additive interstitial space. Qualitatively, the model parameters are the same for ATH and 2CX but the same parametric values involve different *TIR* patterns.

Parametric values of reference for both models were taken from Schabel et al., [31] except for the blood volume which was multiplied by 2 to enhance the difference between models. The resulting parameters were blood flow= 100 mL/100 mL/min, blood volume fraction = 30%, permeability-surface product = 72 mL/100 mL/min and interstitial volume fraction = 25%. Then, TIC was generated by convolving the AIF with *TIRs* generated by both models. For generalization, various sets of parameters around initial parametric values were used to generate data. Moreover, the resulting *TIC* curves were polluted by adding random noise. More precisely, we generated 50 datasets both with 2CX and ATH models, without and with random Gaussian white noise, with a signal to noise ratio of 20. For each case, the initial parametric values were generated randomly by using white homogeneous noise, resulting in parameters varying from half to twice the initial parametric values.

2.3.2 Evaluation of the *TIR* assessments

2CX and ATH *TIC*-curves were analyzed with the FTPH and B-spline models resulting in estimated *TIR* signals. Quantitatively, the accuracy of the deconvolution techniques was evaluated by calculating the mean squared error (QE) which derives from the difference between initial and the estimated *TIR* signals. QE was normalized by the amplitude in the initial *TIR* signal. Then, the quality of the *TIR* estimation was evaluated by testing the ability of several users to identify patterns in the estimated *TIR* signal, enabling the identification of the model used to generate data. This test was established to assess the ability of the FTPH model to be used to identify the pharmacokinetic hypotheses which are more consistent with the observed kinetics. Five observers with different levels of experience in DCE data, blinded from the models, were selected. Impulse responses, estimated by FTPH and B-Splines models, were shown to each observer independently in a random order, on a dedicated in-house reading software developed in Matlab (Mathworks, Natick, MA). Five possible answers corresponding to pattern recognition were proposed: “definite ATH”, “probably ATH”, “undetermined”, “probably 2CX”, and “definite 2CX”. Then, concordance tables were generated by comparison with the model used to generate data, resulting in sensitivity-specificity evaluations by merging «probable» and «definite» model detections. The level of confidence was evaluated as the percentage of the correct evaluation

established as ‘definite’ by the users, and reversely, the level of misleading was defined as the percentage of errors in evaluation despite a ‘definite’ assessment by the readers.

Finally, we evaluated the number of kinetics required to identify correctly the model matching the DCE data. This was performed for the data generated by each model, according to the following decision criterion: «the parametric model (ATH or 2CX) is identified, after k observations, if this model was identified for the majority of the k TIR estimation technique (FTPH or B-Splines) ». The power of decision was evaluated by calculating the number of observations required for the algorithm to identify correctly the model in more than 95% of cases. To perform this step, sets of k pairs (true model, observer identification) were selected randomly for a fixed model, then each observer decision was evaluated as right or wrong. For a given model and a k value, the process was iterated 100 times and the percentage of the correct decision was collected. This process was repeated for all the parametric models (ATH and 2CX), deconvolution techniques (B-Spline, FTPH) and for increasing k values until the proportion of correct k -decisions exceed 95%, then k was selected as a reasonable exam number to identify properly the model in line with the data. The algorithm was stopped for $k=16$, considering that it is not reasonable to expend more than 16 exams to select a pharmacokinetic model for the DCE analysis. The whole process was performed for noisy and noise-free data for each observer and pooled into synthetic tables.

Differences between methods were evaluated with the non-parametric Wilcoxon test. The significance criterion used was $P>0.05$.

2.4 Deconvolution on few real case studies

To illustrate the performance of the FTPH model under real conditions, deconvolution was also tested on 4 experimental datasets: two datasets on regions with expected intravascular CA distribution (brain and placenta), and two datasets with specific micro-circulation (cortical and cortico-medullary parts of the kidney). The spatial delineation of regions of interest and baseline definitions (time before injection) were performed interactively with software developed in Matlab (Mathworks, Natick, MA) [38]. Conversion from signal to concentration assumed a simple linear relationship for simplification. Patient MRIs were selected randomly in clinical studies with principal investigators’ authorization.

3 RESULTS

3.1 Illustration on simulated case studies

The AIF used in simulations is shown in Fig 3.a with the corresponding TIC provided after convolution using 2CX and ATH models, with parametric values given as reference. The corresponding “true” TIR curves were drawn in Fig.3.b and c, as plain curves, for two time scales. The estimated TIR curves provided by deconvolution with the FTPH model were drawn in green in Fig.3.b and c, for both 2CX and ATH. The corresponding TIC curves, resulting from convolution with the AIF , were drawn with green crosses in Fig.3.a. In this visual example, the accuracy of the FTPH fitting was high whatever the model used to generate data (Fig.3.a). The absence of bias and noise in the TIR curves estimated by the FTPH model enables the identification of the patterns corresponding to ATH and 2CX (plateau and maximal initial decrease respectively) see Fig.3.b and c.

3.2 Identification of microcirculation hypothesis

In total, 200 TIR curves were generated (two models, with and without noise). TIR curves were estimated both with FTPH and B-spline, from the AIF and TIC curves. Fig. 4 illustrates deconvolution results for one 2CX data and one ATH data selected randomly from TIR initializations (same parameters). FTPH (in left) estimated accurately the TIR curve whatever the model under evaluation, with and without moderate noise. Conversely, in this example, (Fig. 4, right panel) B-Spline was able to estimate accurately only non-noisy 2CX data, showing otherwise oscillations or loss of the initial plateau from the initial ATH TIR curve.

The five readers selected for model identification were: one radiologist working in an independent DCE study, one engineer in scientific processing with more than 15 years of experience in DCE, one biostatistician, one biologist and one engineering student with no experience in DCE data. Each reader received indications concerning patterns to identify 2CX and ATH models. The model identification based on the FTPH deconvolutions was efficient with mean sensitivity and specificity over 90% for non-noisy data. For noisy data, a moderate loss of efficiency was evaluated, with mean values over 80% (from 80% to 86%). Model identification based on B-Spline was less efficient. First, in line with Fig. 4, sensitivity was low (61%) for ATH detection and high (97%) for 2CX, resulting in a clear asymmetry in the visual interpretation. Specificity was intermediate (75%). The dissymmetry was increased by noise providing a very low sensibility of ATH detection (52%) and a moderate specificity of 2CX detection. All sensitivity-specificity values were collected in Table 2.

The number of exams required to establish a reliable model identification (95% of confidence) was computed and collected shown in Table 3. Globally, the number of examinations required for the evaluation was substantially lower with FTPH than with B-Spline. For FTPH, few data ($n < 4$) were required for the model identification. This number increased moderately with noise ($n < 9$). For B-Splines, the efficiency of model detection depended clearly on the model ($n < 5$ for 2CX and $n > 16$ for ATH), which confirms its non-neutrality.

Additionally, the level of confidence of the readers in their evaluations increased from B-Splines to FTPH, from 61% to 77% ($p = 0.056$, Wilcoxon) without noise, and from 30% to 60% with noise ($P < 0.01$, Wilcoxon), respectively. The level of misleading of readers decreased from B-Splines to FTPH, from 13% down to 0.8% without noise ($P < 0.01$, Wilcoxon) and from 9% down to 7% with noise (NS), respectively.

3.3 Quantitative evaluation (see Table 4)

For 2CX data without noise, both mean squared errors were low ($QE < 2.6\%$) regardless of the deconvolution model. In other cases, modeling QEs were lower for FTPH than for B-Spline which provided QE of 25% for 2CX and 45% for ATH with noise. Regarding the FTPH modeling, QE was contained under 10% even with the noise. Differences in values found between FTPH and B-Splines were confirmed with Wilcoxon tests ($P < 5.10^{-5}$). Also, for FTPH, QEs were comparable whatever the model used to generate data ($P > 0.05$) whereas for B-Splines, QE was higher for data generated by the ATH model ($P < 5.10^{-5}$).

3.4 Case studies on real data

3.4.1 Exploration

The FTPH model provided fitted *TIC* curves which were consistent with enhancements observed in the brain and kidney, as shown in the right panels of Fig. 5. In all tissues of interest, the fitting of *TIC* was regular and faithful regarding the shape of the signals measured. This suggested good compliance of the model according to different acquisition contexts. Moreover, *TIR* curves, on the left, which were estimated from AIF and *TIC*, were both sharp and regular, i.e. compatible both with accuracy and precision. The shapes of the estimated *TIR* curves in the brain, without any visible plateau, suggested a poor agreement with the ATH hypothesis. It suggests that ATH should therefore be avoided to interpret this type of data physiologically. The shapes of the estimated *TIR* curves in the kidney, indicated an initial decrease with an intermediate pattern between the 2CX and ATH models that could be compatible with the Schabel model [31]. Plateaus around 80 seconds suggested ATH-like behavior, but, unexpectedly, for tubular microcirculation. [For placental data, the comparison between ATH and 2CX curves is shown in more detail in Fig. 6.](#)

3.4.2 Comparison

FTPH modeling was also compared to 2CX and ATH modeling on placental data, as shown in Fig. 6. TICs indicate that the ATH model provided a poorer fit than 2CX and FTPH models. Qualitatively, the fits of 2CX and FTPH were very accurate. Comparison of impulse responses indicates that 2CX and FTPH provided nearly equal TIRs. The exponential hypothesis, considered a priori by the 2CX model, was confirmed after by the FTPH model as an output of the data. This TIR equality suggested an absence of indetermination. Indeed, the 2CX and FTPH models being independent, if there were several equivalent micro-circulatory hypotheses or TIR patterns to explain the measured TIC equivalently, it would have been unlikely that the two models would converge towards the same solution.

4 DISCUSSION

The accuracy and precision of the FTPH model to assess TIRs were confirmed in a framework of simulated data. Mean squared errors lower than 10% were found in the data generated by the two 2CX and ATH models. This error, including bias and noise, was small enough to allow observers to identify the tissue microcirculation assumption underlying their data, regardless of the initial microcirculatory assumption. Moreover, results performed on several clinical data suggested that the FTPH model could be used for a larger scope of acquisitions. Overall, these results show the potential of the FTPH model for describing various DCE datasets neutrally and accurately.

A correct DCE data description is not limited to a correct description of tissue observation (TIC). TIC provides only information on the evolution of the amount of contrast agent in the tissue, following injection. The transition between the entry of the contrast agent into the tissue (AIF) and its presence over time (TIC) depends on the mobility of the contrast agent within the different tissue structures, i.e. on the tissue microcirculation. As it is widely accepted that this transition can be expressed as a convolution with a tissue impulse response (TIR), TIR is assumed to be a correct description of the DCE data (the AIF, TIC pair). Thus, TIR contains the microcirculatory information; it is accessible only as data derived from AIF and TIC; and it is a common component of all deconvolution models. This consideration explains respectively (i) why we tried to evaluate properly TIR with our model and not TICs as is more commonly performed [24], (ii) why we evaluated the descriptive capabilities of our model not directly

on data but rather on TIRs which were assumed to be known thanks to simulations, (iii) and why a correct assessment of the TIR with a model such as the FTPH can be used as a reference for any PK model.

The main innovation of the FTPH model versus B-Spline, was the introduction of construction points with variable time steps. This property allows the model to focus on the data description where the information is located. Beyond the simple technical aspect, this allowed us to remove an implicit hypothesis from the original B-Spline model that limited its scope. In the original model, the homogeneous sampling of the construction points (data features) assumes that the TIR information is distributed homogeneously over time. Technically, it induces a cut-off frequency and, therefore, homogeneous smoothing. However, theoretically, the minimum-hypothesis model does not contain this assumption. This produces a mismatch between the theoretical model and its numerical transcription. As this mismatch is based on technical considerations, this issue is particularly difficult to identify from a final user specialized in physiological or medical issues. Moreover, the B-Splines model does not strictly verify the decay hypothesis, as shown by the oscillations in Fig. 4 B. This second drift was corrected with the FTPH model. Thus, thanks to a more faithful numerical transcription of the theoretical minimal-hypothesis model, we have improved the control over a technical tool, simplified its formulation and then improved its TIR assessment efficiency. Theoretically, the minimal-hypothesis model only indicates that (1) the number of data features (model dimension) must be moderate because not all the measurements are independent, and (2) TIR is a decreasing function. Conventional deconvolution techniques are based on linear regularization methods, which are based on efficient signal processing techniques, but their relationship with the simple theoretical minimal-hypothesis model remains unclear. This concerns especially the regularization process, for the definition of the regularity metrics and the settings of the weighting between regularity and accuracy [32]. The consequences concerning the mismatch between the numerical and the theoretical model are more difficult to establish than with a simple sampling. This may explain why, to our knowledge, no TIR assessment has been proposed even though deconvolution techniques have been used in DCE for years [39].

Most of the previous studies in the literature had as main objective to retrieve sufficient information to classify patients. [In this case, the search for information is subjected to a compromise because the needs are related to capture information, provide stable results, and provide results sufficiently synthetic to facilitate a decision-making process.](#) Interestingly, not all physiological information is necessarily useful to identify the stage of pathology. It has even been shown that refining the description of TIRs by complex models could be detrimental to the discriminant capacity of the classification [11]. This explains why the simple Tofts-Kety model is currently used in oncology rather than the more physiological but more complex 2CX or ATH models [13]. With conventional parametric models, the TIRs assessment is voluntarily roughly approximate to ensure good robustness of the results. Thus, it is not necessary to describe the AIF/TIC transition in full detail to provide a diagnosis. Without reliable measurement or assessment of AIF, investigators should even be limited to the descriptive analyses of TICs. Indeed, in some cases, it was possible to discriminate pathological statuses using TIC descriptions only, assuming that AIFs were close between patients, or assuming that TICs could be compared to another internal reference tissues [40,41]. However, with these approaches, the link with microcirculation remains vague. This is why most investigators use convolution models. Overall, with conventional methods, the risks of bias are usually tolerated to reduce the risk of instability as much as possible, in order to improve inter-patient and inter-center reproducibility [16,18,27]. This approach is consistent as long as the DCE analysis is used as a black box. However, if the parameters of the DCE models need to be interpreted in terms of tissue microcirculation, approximations and partial descriptions become an issue. However, attempts at interpretation from PK models are not uncommon [5,19], even when the models were not designed for this purpose. Information criteria were developed in line with the conventional classification challenge. The Bayesian and Akaike-type criteria: BIC, AIC, AICc and F-Test [12,13,24–26] were addressed to assess the

"quality" of DCE models used for data fitting. They derive from TIC and measure the performance of information retrieval. The performance increases with the integration of information into the model representation and decreases with the number of parameters required to establish this representation. These criteria propose an "ideal balance" between information retrieval and risk of instability, in accordance with the objective of classification [44]. Indeed, the more information available, the easier it will be to discriminate between groups of patients. Conversely, the more parameters are provided, the less this information will be usable by classification systems. However, these comparative criteria only provide a scale of appreciation between different models [24]. They do not indicate the performance of the best of the models tested in terms of agreement with data. Then, they do not determine whether a model is sufficiently consistent with the data to be considered as a valid physiological explanation of the observed data.

When DCE data are fitted with a model, this model provides three results: a set of parameters $\{p\}$; the corresponding parameterized impulse response ($TIR(t, \{p\})$) and the TIC assessment (TIC_a) obtained by convolving TIR with AIF. The set of parameters $\{p\}$ corresponds to a *synthesis* of the information needed to build TIR. If the parameters are *interpreted* in physiological terms, they are also used to *explain* TIR, thus explaining the pharmacokinetic transition from AIF to TIC. TIR itself, considered as a signal, regardless of the formulation used to perform its calculation, is a simple *description* of the transition from AIF to TIC. TIC_a is a by-product of AIF and the assessed TIR. It does not directly carry the pharmacokinetic information but can be directly compared to the measured tissue response. The Bayesian and Akaike-type criteria are based on the evaluation of the differences between the estimated and the observed TIC. Another approach was previously proposed to evaluate the TIC gap: the Fraction of Modeling Information (FMI), which was renormalized with the Fraction of Lasting Information (FLI) [22,24]. While the Akaike criteria compares the TIC error to the model dimension, the FMI criteria compares the total TIC error with the basic TIC error resulting only from the noise magnitude. The difference is the modeling error, which corresponds to the discrepancy between the model and the data that the model claims to explain. However, FMI, as Akaike-type criteria, is based on TIC analysis. It is thus AIF-dependent, and therefore less informative than an analysis performed on TIRs. Moreover, the FMI is a scalar that does not allow us to appreciate the nature of the mismatch between modeling and measurement. [It would therefore be interesting to have criteria based on TIRs to complement the tools already available that are based on TIC analysis.](#)

In our study, we used the FTPH model to describe TIR in a way that was both parsimonious and as neutral as possible. The objective was to have an optimized tool for the *description* of the transition from AIF to TIC, without constraints imposed either by synthesis requirements (parametric models) or by technical tools that are challenging to control well (usual nonparametric models). However, the TIR assessment is challenging. The convolution with the AIF acts as a low pass-filter which can reduce differences between TICs from differences that could appear more clearly in TIR curves. The advantage of TIR is that it derives directly from the pharmacokinetic information being sought. The concern is that there is no baseline measure available to know the "true observed TIR". We, therefore, tested the FTPH model efficiency from known simulated TIRs. Complex and divergent models were used for the simulation to test the FTPH model under a variety of non-trivial experimental conditions. The agreement between the FTPH model and our data was high. And indeed, the FTPH model allowed even inexperienced users to evaluate the type of microcirculation that was in agreement with their data. To our knowledge, this capability has not been reported for any other model. [Thus, although the "true TIR" is not directly measurable from the data \(AIF, TIC\), our results suggest that the FTPH model is a viable model to provide a satisfactory assessment of this curve \(agreement with the data\). In](#)

other words, the FTPH model was a *viable* descriptive reference model (DRM) of DCE data, which verifies our original hypothesis.

Assuming that the FTPH model can be considered a DRM under most of the experimental conditions (which remains to be demonstrated), the FTPH model would provide means of evaluating the agreement between any PK model and any new DCE dataset by comparing TIR_{PK} and TIR_{FTPH} . This comparison was performed when we analyzed the real data by comparing TIR_{FTPH} to the expected or calculated shapes of TIR_{PK} , for PK equals 2CX and ATK respectively. It suggested for instance that a 2CX-type model should be more appropriate than an ATH-type model for analyzing cerebral and placental data if physiological indications are to be drawn from it. In the simulation analysis, we evaluated quantitatively the agreement between the FTPH model and the ground truth generated by the 2CX and ATH models, using the mean squared error between TIR_{FTPH} and TIR_{PK} , where PK corresponded either to ATH or 2CX. On new data, where the microcirculatory assumptions are poorly established, the same logic can be applied but in the other direction: the model to be tested is the PK model and the ground truth corresponds to the FTPH model which is assumed to be a DRM. The agreement still consists of a calculation of the mean squared error between TIR_{PK} and TIR_{FTPH} . However, these are only conditional perspectives on the fact that the FTPH model remains a reference model in a broader context than that of our study. Furthermore, it should be noted that consistency between modeling and observations is a necessary condition for the interpretation of pharmacokinetic parameters (TIR_{PK} with TIR_{DRM}). But the descriptive capacity of TIR_{PK} does not guarantee the explanatory capacity of the $\{p\}$, used to define TIR, in terms of physiology. For this, the previous internal controls have to be completed by validation studies [42,43]. However, this is out of the scope of our study.

Parametric PK models and the FTPH model do not have the same function. PK models have to simultaneously meet several objectives: to be stable, to extract essential information, to provide synthetic and if interpretable results. Their ability to address these various properties globally makes PK models useful from a technical point of view, especially for classification. However, these multiple functionalities generally make them unsuitable for performing one function optimally, independently of their other functions. In particular, they are not optimal for describing accurately DCE data. Thus, they usually describe the DCE data more or less roughly. On the contrary, the FTPH model was designed to specifically address this concern. It is expected to fulfill this function better than the KP models, and it is, therefore, likely to serve as a reference in this field. Conversely, it does not provide an easily manipulated synthesis and does not bring any interpretation except the minimal assumption of a convolution. The FTPH model is, therefore, a complementary tool to the standard models

Different limitations were identified concerning both the FTPH model and the challenge designed to test its performances. *First*, this initial study had a limited scope. The evaluation concerned limited types of data (2CX and ATH), with limited levels of noise. Few evaluation criteria were used in simulated data and the evaluations on measured data were just use-cases, for illustrative purposes only. However, a wider generalization is beyond the scope of this initial study. We have already shown that the search for a well-conditioned deconvolution method is possible in DCE, which opens interesting perspectives to better explore microcirculation in-vivo or to better estimate the interpretative value of current PK models. *Second*, the optimization technique used to fit the data with the FTPH model was not completely explored. For simplification, a current method available in our laboratory was used. Alternative algorithms were not explored nor the impact of parametric initialization and so on. *Third*, the generality of the FTPH model presented here should be further improved. For simplicity, six points were chosen to test the FTPH model. An adaptive technique should be considered to dimension the model according to the level of information available in the data. Moreover, the input function in the tissue should not be equal but derive from the AIF measured upstream

in a large artery. Then a short period of growth could be allowed before imposing the main decrease in the FTPH model, to include the dispersion of the contrast agent from the large artery to the tissue input, and thus make the model compatible with gamma variate patterns. *Fourth*, any model including convolution assumes that a correct measurement of arterial input is available. However, a correct measurement of AIF can be experimentally complicated. In this case, we recommend not to interpret the obtained parameters. Similarly, we have assumed that the various signal distortions and other artifacts, which are the subject of other publications [27], are either minor or corrected.

5 CONCLUSION

The free-time-point-Hermite model constitutes a direct and robust model to describe the *TIR* curves. It employs the localization of a few mobile construction-points defined in abscissa and ordinate, combined with an adequate interpolation and a direct decreasing constraint. Our results suggest that such a tool can be used to explore the microcirculatory structure expressed in DCE data. More generally, access to well-conditioned deconvolution techniques is likely to serve as a reference *TIR* for estimating the interpretative value of conventional PK models, and to explore data with a minimal hypothesis, so that the observer can be guided in the formulation of new pharmacokinetic hypotheses.

Acknowledgments

FTPH evaluation was possible in patient data thanks to the agreements of principal investigators of several studies that are namely Nathalie Siauve, Catherine Lefort and Laure Fournier. Thanks to Thomas Viel for improving the readability of the paper.

REFERENCES

- [1] K.V. Lund, T.G. Simonsen, G.B. Kristensen, E.K. Rofstad, Pharmacokinetic analysis of DCE-MRI data of locally advanced cervical carcinoma with the Brix model, *Acta Oncologica*. 58 (2019) 828–837. <https://doi.org/10.1080/0284186X.2019.1580386>.
- [2] G. Dodin, J. Salleron, S. Jendoubi, W. Abou Arab, F. Sirveaux, A. Blum, P.A. Gondim Teixeira, Added-value of advanced magnetic resonance imaging to conventional morphologic analysis for the differentiation between benign and malignant non-fatty soft-tissue tumors, *Eur Radiol*. (2020). <https://doi.org/10.1007/s00330-020-07190-0>.
- [3] C. Hayes, A.R. Padhani, M.O. Leach, Assessing changes in tumour vascular function using dynamic contrast-enhanced magnetic resonance imaging, *NMR in Biomedicine*. 15 (2002) 154–163. <https://doi.org/10.1002/nbm.756>.
- [4] Z. Liu, B. Feng, C. Li, Y. Chen, Q. Chen, X. Li, J. Guan, X. Chen, E. Cui, R. Li, Z. Li, W. Long, Preoperative prediction of lymphovascular invasion in invasive breast cancer with dynamic contrast-enhanced-MRI-based radiomics, *J Magn Reson Imaging*. 50 (2019) 847–857. <https://doi.org/10.1002/jmri.26688>.
- [5] M. Claudon, E. Durand, N. Grenier, A. Prigent, D. Balvay, P. Chaumet-Riffaud, K. Chaumoitre, C.-A. Cuenod, M. Filipovic, M.-A. Galloy, L. Lemaitre, D. Mandry, E. Micard, C. Pasquier, G.H. Sebag, M. Soudant, P.-A. Vuissoz, F. Guillemin, DCE MR Urography Study Group, Chronic urinary obstruction: evaluation of dynamic contrast-enhanced MR urography for measurement of split renal function, *Radiology*. 273 (2014) 801–812. <https://doi.org/10.1148/radiol.14131819>.
- [6] M. Fan, P. Zhang, Y. Wang, W. Peng, S. Wang, X. Gao, M. Xu, L. Li, Radiomic analysis of imaging heterogeneity in tumours and the surrounding parenchyma based on unsupervised decomposition of DCE-MRI for predicting molecular subtypes of breast cancer, *Eur Radiol*. 29 (2019) 4456–4467. <https://doi.org/10.1007/s00330-018-5891-3>.
- [7] K. Sun, H. Zhu, W. Chai, Y. Zhan, D. Nickel, R. Grimm, C. Fu, F. Yan, Whole-lesion histogram and texture analyses of breast lesions on inline quantitative DCE mapping with CAIPIRINHA-Dixon-TWIST-VIBE, *Eur Radiol*. 30 (2020) 57–65. <https://doi.org/10.1007/s00330-019-06365-8>.
- [8] B. Turkbey, P.L. Choyke, PIRADS 2.0: what is new?, *Diagn Interv Radiol*. 21 (2015) 382–384. <https://doi.org/10.5152/dir.2015.15099>.

- [9] K. Pinker, L. Moy, E.J. Sutton, R.M. Mann, M. Weber, S.B. Thakur, M.S. Jochelson, Z. Bago-Horvath, E.A. Morris, P.A. Baltzer, T.H. Helbich, Diffusion-weighted Imaging with Apparent Diffusion Coefficient Mapping for Breast Cancer Detection as a Stand-Alone-Parameter: Comparison with Dynamic Contrast-enhanced and Multiparametric Magnetic Resonance Imaging, *Invest Radiol.* 53 (2018) 587–595. <https://doi.org/10.1097/RLI.0000000000000465>.
- [10] L. Desquilbet, Guide pratique de validation statistique de méthodes de mesure : répétabilité, reproductibilité, et concordance, (n.d.) 47.
- [11] C. Duan, J.F. Kallehauge, G.L. Bretthorst, K. Tanderup, J.J.H. Ackerman, J.R. Garbow, Are complex DCE-MRI models supported by clinical data?, *Magnetic Resonance in Medicine*. 77 (2017) 1329–1339. <https://doi.org/10.1002/mrm.26189>.
- [12] J.P.B. O'Connor, A. Jackson, G.J.M. Parker, G.C. Jayson, DCE-MRI biomarkers in the clinical evaluation of antiangiogenic and vascular disrupting agents, *British Journal of Cancer*. 96 (2007) 189–195. <https://doi.org/10.1038/sj.bjc.6603515>.
- [13] A. Shukla-Dave, N.A. Obuchowski, T.L. Chenevert, S. Jambawalikar, L.H. Schwartz, D. Malyarenko, W. Huang, S.M. Noworolski, R.J. Young, M.S. Shiroishi, H. Kim, C. Coolens, H. Laue, C. Chung, M. Rosen, M. Boss, E.F. Jackson, Quantitative imaging biomarkers alliance (QIBA) recommendations for improved precision of DWI and DCE-MRI derived biomarkers in multicenter oncology trials, *Journal of Magnetic Resonance Imaging*. 49 (2019) e101–e121. <https://doi.org/10.1002/jmri.26518>.
- [14] S.P. Sourbron, D.L. Buckley, Tracer kinetic modelling in MRI: estimating perfusion and capillary permeability, *Phys. Med. Biol.* 57 (2011) R1–R33. <https://doi.org/10.1088/0031-9155/57/2/R1>.
- [15] L. Beuzit, P.-A. Eliat, V. Brun, J.-C. Ferré, Y. Gandon, E. Bannier, H. Saint-Jalmes, Dynamic contrast-enhanced MRI: Study of inter-software accuracy and reproducibility using simulated and clinical data, *Journal of Magnetic Resonance Imaging*. 43 (2016) 1288–1300. <https://doi.org/10.1002/jmri.25101>.
- [16] T. Heye, M.S. Davenport, J.J. Horvath, S. Feuerlein, S.R. Breault, M.R. Bashir, E.M. Merkle, D.T. Boll, Reproducibility of dynamic contrast-enhanced MR imaging. Part I. Perfusion characteristics in the female pelvis by using multiple computer-aided diagnosis perfusion analysis solutions, *Radiology*. 266 (2013) 801–811. <https://doi.org/10.1148/radiol.12120278>.
- [17] N.A. Pack, E.V.R. DiBella, Comparison of Myocardial Perfusion Estimates From Dynamic Contrast-Enhanced Magnetic Resonance Imaging With Four Quantitative Analysis Methods, *Magn Reson Med*. 64 (2010) 125–137. <https://doi.org/10.1002/mrm.22282>.
- [18] T. Niu, P. Yang, X. Sun, T. Mao, L. Xu, N. Yue, Y. Kuang, L. Shi, K. Nie, Variations of quantitative perfusion measurement on dynamic contrast enhanced CT for colorectal cancer: implication of standardized image protocol, *Phys. Med. Biol.* 63 (2018) 165009. <https://doi.org/10.1088/1361-6560/aac699>.
- [19] H.J. van de Haar, S. Burgmans, J.F.A. Jansen, M.J.P. van Osch, M.A. van Buchem, M. Muller, P.A.M. Hofman, F.R.J. Verhey, W.H. Backes, Blood-Brain Barrier Leakage in Patients with Early Alzheimer Disease, *Radiology*. 281 (2016) 527–535. <https://doi.org/10.1148/radiol.2016152244>.
- [20] J. Nickander, R. Themudo, A. Sigfridsson, H. Xue, P. Kellman, M. Ugander, Females have higher myocardial perfusion, blood volume and extracellular volume compared to males – an adenosine stress cardiovascular magnetic resonance study, *Scientific Reports*. 10 (2020) 10380. <https://doi.org/10.1038/s41598-020-67196-y>.
- [21] H. Everaars, P.A. van Diemen, M.J. Bom, S.P. Schumacher, R.W. de Winter, P.M. van de Ven, P.G. Raijmakers, A.A. Lammertsma, M.B.M. Hofman, R.J. van der Geest, M.J. Götte, A.C. van Rossum, R. Nijveldt, I. Danad, R.S. Driessen, P. Knaapen, Comparison between quantitative cardiac magnetic resonance perfusion imaging and [15O] H₂O positron emission tomography, *Eur J Nucl Med Mol Imaging*. 47 (2020) 1688–1697. <https://doi.org/10.1007/s00259-019-04641-9>.
- [22] D. Balvay, F. Frouin, G. Calmon, B. Bessoud, E. Kahn, N. Siauve, O. Clément, C.A. Cuenod, New criteria for assessing fit quality in dynamic contrast-enhanced T1-weighted MRI for perfusion and permeability imaging, *Magn Reson Med*. 54 (2005) 868–877. <https://doi.org/10.1002/mrm.20650>.
- [23] T. Gaa, W. Neumann, S. Sudarski, U.I. Attenberger, S.O. Schönberg, L.R. Schad, F.G. Zöllner, Comparison of perfusion models for quantitative T1 weighted DCE-MRI of rectal cancer, *Sci Rep*. 7 (2017) 1–9. <https://doi.org/10.1038/s41598-017-12194-w>.
- [24] A. Lecler, D. Balvay, C.-A. Cuenod, L. Marais, M. Zmuda, J.-C. Sadik, O. Galatoire, E. Farah, J.E. Methni, K. Zuber, O. Bergès, J. Savatovsky, L. Fournier, Quality-based pharmacokinetic model selection on DCE-MRI for characterizing orbital lesions, *Journal of Magnetic Resonance Imaging*. 50 (2019) 1514–1525. <https://doi.org/10.1002/jmri.26747>.
- [25] N. Dikaio, D. Atkinson, C. Tudisca, P. Purpura, M. Forster, H. Ahmed, T. Beale, M. Emberton, S. Punwani, A comparison of Bayesian and non-linear regression methods for robust estimation of pharmacokinetics in DCE-MRI and how it affects cancer diagnosis, *Computerized Medical Imaging and Graphics*. 56 (2017) 1–10. <https://doi.org/10.1016/j.compmedimag.2017.01.003>.
- [26] M. Lowry, B. Zelhof, G.P. Liney, P. Gibbs, M.D. Pickles, L.W. Turnbull, Analysis of prostate DCE-MRI: comparison of fast exchange limit and fast exchange regimen pharmacokinetic models in the discrimination of malignant from normal tissue, *Invest Radiol*. 44 (2009) 577–584. <https://doi.org/10.1097/RLI.0b013e3181b4c1fe>.
- [27] H. Kim, Variability in Quantitative DCE-MRI: Sources and Solutions, *J Nat Sci*. 4 (2018). <https://www.ncbi.nlm.nih.gov/pmc/articles/PMC5841165/> (accessed March 24, 2020).
- [28] C.A. Cuenod, D. Balvay, Perfusion and vascular permeability: basic concepts and measurement in DCE-CT and DCE-MRI, *Diagn Interv Imaging*. 94 (2013) 1187–1204. <https://doi.org/10.1016/j.diii.2013.10.010>.

- [29] M. Jerosch-Herold, C. Swingen, R.T. Seethamraju, Myocardial blood flow quantification with MRI by model-independent deconvolution, *Med. Phys.* 29 (2002) 886–897. <https://doi.org/10.1118/1.1473135>.
- [30] H. Prautzsch, W. Boehm, M. Paluszny, Bézier and B-spline techniques, Springer, New York, NY, 2002.
- [31] M.C. Schabel, A unified impulse response model for DCE-MRI: A Unified Impulse Response Model for DCE-MRI, *Magnetic Resonance in Medicine*. 68 (2012) 1632–1646. <https://doi.org/10.1002/mrm.24162>.
- [32] P.C. Hansen, REGULARIZATION TOOLS: A Matlab package for analysis and solution of discrete ill-posed problems, *Numerical Algorithms*. 6 (1994) 1–35. <https://doi.org/10.1007/BF02149761>.
- [33] S. Sourbron, R. Luyt, P.V. Schuerbeek, M. Dujardin, T. Stadnik, M. Osteaux, Deconvolution of dynamic contrast-enhanced MRI data by linear inversion: Choice of the regularization parameter, *Magnetic Resonance in Medicine*. 52 (2004) 209–213. <https://doi.org/10.1002/mrm.20113>.
- [34] K. Murase, Y. Yamazaki, S. Miyazaki, Deconvolution analysis of dynamic contrast-enhanced data based on singular value decomposition optimized by generalized cross validation, *Magn Reson Med Sci*. 3 (2004) 165–175.
- [35] M. Jerosch-Herold, C. Swingen, R.T. Seethamraju, Myocardial blood flow quantification with MRI by model-independent deconvolution, *Medical Physics*. 29 (2002) 886–897. <https://doi.org/10.1118/1.1473135>.
- [36] Solve nonlinear curve-fitting (data-fitting) problems in least-squares sense - MATLAB lsqcurvefit - MathWorks France, (n.d.). https://fr.mathworks.com/help/optim/ug/lsqcurvefit.html?searchHighlight=lsqcurvefit&s_tid=doc_srchtile (accessed July 12, 2017).
- [37] I. Thomassin-Naggara, N. Soualhi, D. Balvay, E. Darai, C.-A. Cuenod, Quantifying tumor vascular heterogeneity with DCE-MRI in complex adnexal masses: A preliminary study, *J Magn Reson Imaging*. (2017). <https://doi.org/10.1002/jmri.25707>.
- [38] D. Balvay, I. Tropès, R. Billet, A. Joubert, M. Péoc'h, C.A. Cuenod, G. Le Duc, Mapping the Zonal Organization of Tumor Perfusion and Permeability in a Rat Glioma Model by Using Dynamic Contrast-enhanced Synchrotron Radiation CT ¹, *Radiology*. 250 (2009) 692–702. <https://doi.org/10.1148/radiol.2501071929>.
- [39] Z. Szabó, G. Torsello, C. Reifenrath, R. Porschen, H. Vosberg, [An experimental study of liver perfusion using non-diffusible radiotracers: differentiation of the arterial and portal venous components by deconvolution analysis of first-pass time-activity curves], *Nuklearmedizin*. 27 (1988) 209–218.
- [40] I. Thomassin-Naggara, D. Balvay, C.A. Cuenod, E. Daraï, C. Marsault, M. Bazot, Dynamic contrast-enhanced MR imaging to assess physiologic variations of myometrial perfusion, *Eur Radiol*. 20 (2010) 984–994. <https://doi.org/10.1007/s00330-009-1621-1>.
- [41] D. Ippolito, S.G. Drago, A. Pecorelli, C. Maino, G. Querques, I. Mariani, C.T. Franzesi, S. Sironi, Role of dynamic perfusion magnetic resonance imaging in patients with local advanced rectal cancer, *World J. Gastroenterol*. 26 (2020) 2657–2668. <https://doi.org/10.3748/wjg.v26.i20.2657>.
- [42] M. Jerosch-Herold, N. Wilke, MR first pass imaging: quantitative assessment of transmural perfusion and collateral flow, *Int J Card Imaging*. 13 (1997) 205–218. <https://doi.org/10.1023/a:1005784820067>.
- [43] Y. Zhao, L. Hubbard, S. Malkasian, P. Abbona, S. Molloy, Dynamic pulmonary CT perfusion using first-pass analysis technique with only two volume scans: Validation in a swine model, *PLoS ONE*. 15 (2020) e0228110. <https://doi.org/10.1371/journal.pone.0228110>.
- [44] R. Paudyal, Y. Lu, V. Hatzoglou, A. Moreira, H.E. Stambuk, J.H. Oh, K.M. Cunanan, D.A. Nunez, Y. Mazaheri, M. Gonen, A. Ho, J.A. Fagin, R.J. Wong, A. Shaha, R.M. Tuttle, A. Shukla-Dave, Dynamic contrast-enhanced MRI model selection for predicting tumor aggressiveness in papillary thyroid cancers, *NMR in Biomedicine*. 33 (2020) e4166. <https://doi.org/10.1002/nbm.4166>.

Table 1. Parameters of the MRI sequences

Table 2. Efficiency of the identification of pharmacokinetic hypotheses. Sensibility and specificity for Hermite and B-spline model to identify data generated with ATH and 2CX assumptions. (presented as mean values with standard deviations)

Table 3. Average number of tests to identify the pharmacokinetic hypothesis. Number of measurements required to identify the initial pattern (2CX or ATH assumptions) with 95% of confidence, with Hermite and B-spline modeling.

Table4. Estimated error of the TIR. Modeling errors (QE in %) between initial impulse responses generated with ATH and 2CX models and Hermite and B-spline estimations, for noisy (SNR = 20) and non-noisy data. Values: means with standard deviation

Figure 1: Graphical representation of the deconvolution models model. **(a)** The B-Spline model is defined by 15 control points which can be modified in amplitude. Their temporal location is homogeneous. The assessed TIR curve is continuously constructed from the control points using the B-Spline technique, including conventional splines. The decay constraint is not imposed directly on the reconstructed curve. **(b)** The FTPH model is defined by 6 reference points included in the final assessed TIR curve which can be modified both in amplitude and time. The decay constraint was imposed on the reference point and propagated by interpolation between these points by using a Hermite's spline.

Figure 2: Assessment of deconvolution models. A measured arterial input function (AIF) was convolved with impulse responses (TIR) generated by two competing DCE models (2CX and ATH), to produce noisy tissue responses (TIC). Then, AIF and TICs were provided to the B-Splines and FTPH deconvolution models that generated an assessment of the initial TIRs (TIRa). The difference between TIRa and TIRs was then evaluated in terms of relative root mean square error and difficulty to visually identify the original model from the observation of the TIRe.

Figure 3: Example of Hermite analysis performed on data generated with 2CX and ATH models for simulated data without noise. **(a)** Data fitting with the Hermite model (green) of data generated with a 2CX (blue) and a ATH (dashed red). The corresponding arterial input function (AIF in dark red) was indicated with its own scale. **(b and c)** Corresponding tissue impulse response (TIR) signals, for the initial time points in **(b)** and all time points in **(c)**. In this example, Hermite enabled a correct fitting of the signal and a correct recovery of initial TIR curves bearing tissue information.

Figure 4: Tissue impulse responses (TIR) from 2CX and ATH data fitted with Hermite and B-spline models, with and without noise. **(Up)** initial 2CX TIC-curve. **(Down)** initial ATH TIC-curve. **(Left)** fitted by Hermite. **(Right)** fitted by B-Spline. In these examples, the TIC assessment by Hermite was correct whatever the model and the noise condition. Oscillations and loss of information are visible for the B-Spline model.

Figure 5: Hermite's model applied on 4 different study cases and for 3 different patients during MRI acquisitions. **(Left)** tissue impulse responses estimated by Hermite. **(Right)** fitting of tissue responses, including enhancements measured in tissues, data fitting with Hermite model, and the difference (crosses): the residue. Line 1 in brain **(a-b)**, and line 2 in placenta **(c-d)**, tissues with intravascular distribution. Line 3 and 4 in kidney: **(e-f)** in a cortical region, **(g-h)** in a cortico medular region. Fittings were consistent for each tissue response. Corresponding unnoisy tissue impulse responses (TIR) provided descriptions which were not in line with the ATH model.

Figure 6. Comparison between the 2CX and ATH parametric models versus the FTPH model. **(Left)** Impulse Responses: TIRs; **(Right)** Tissue Responses: TICs. The TIC curves indicate that the ATH model describes the data (black) more coarsely than the 2CX (blue) and the FTPH model (green). FTPH and 2CX describe TIC correctly. These indications are confirmed in the TIRs, which provide additional information. The differences are more noticeable due to a noise reduction compared to the measurements. Moreover, the nature of the differences can be clarified: the hypothesis of a minimal transit time in the tissue (red plateau) is not confirmed by observation (FTPH data-based model). The 2CX and ATH TIRs overlap, apart from the first point. As the TICs are the result of a convolution of the TIRs with the arterial input (AIF), different TIRs can provide very close TICs. In this case, the "true TIR" is undetermined and several TIRs from different models are plausible, which weakens the interpretative value of each model. In this example this is not the case: two independent models converged to the same TIR,

which suggests that the description provided by the 2CX model is the only one compatible with the observation. The TIR of the 2CX model is therefore in agreement with the data and seems to be imposed by the data itself.

A

B-Splines

- 15 x 1D control-points
- Spline reconstruction
- Homogeneous sampling
- Indirect decay constraint



...

time

B

FTPH

- 6 x 2D reference-points
- Hermite interpolation
- Inhomogeneous sampling
- Direct decay constraint

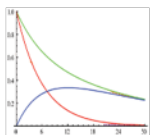


time

Data generation

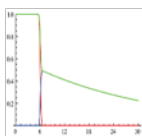
TIR assessment

2CX



TIR_{2CX}

ATH



TIR_{ATH}

(n = 100)

* AIF + Noise = TICs

B-Splines

TIR_a

FTPH

TIR_a

comparison

IR error

Power of identification

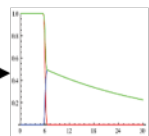
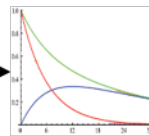
$$E = \frac{\left\| TIR_{(2CX,ATH)} - TIR_{a(Bspline, FTPG)} \right\|^2}{\left\| TIR_{(2CX,ATH)} \right\|^2}$$

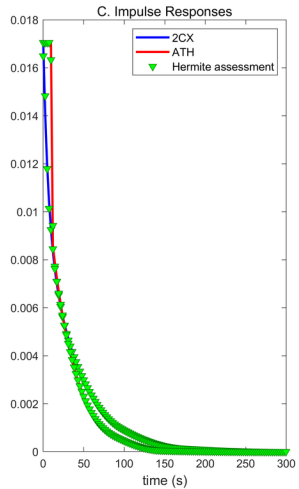
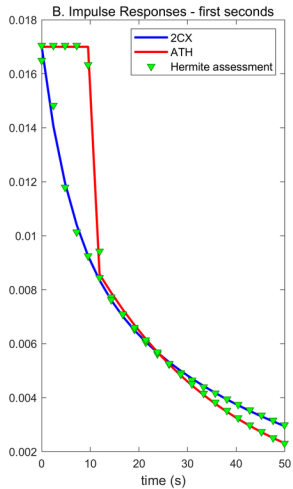
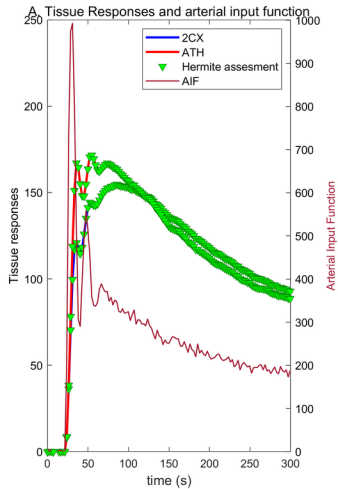
Generated from ?

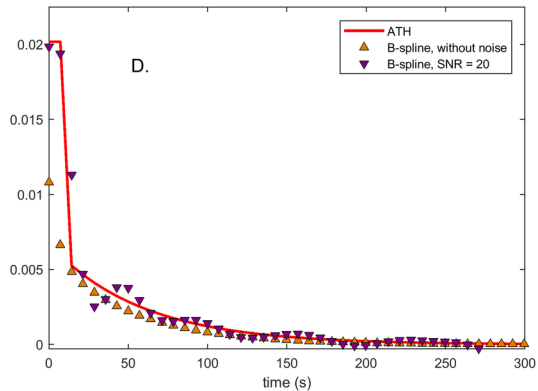
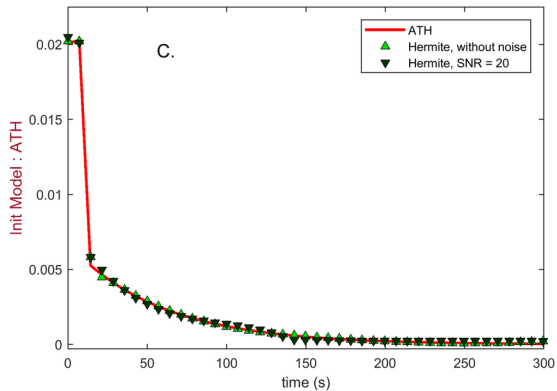
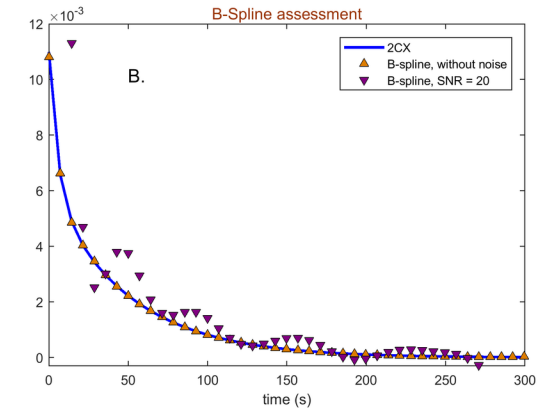
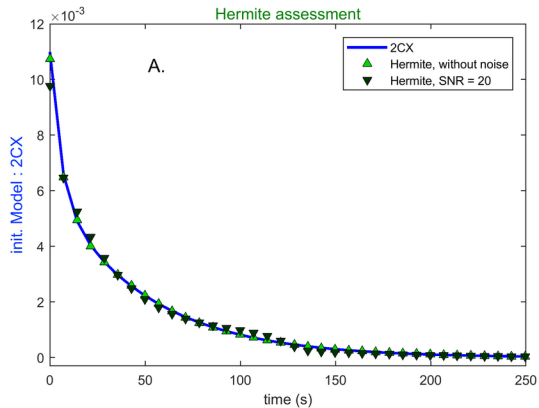
TIR_a

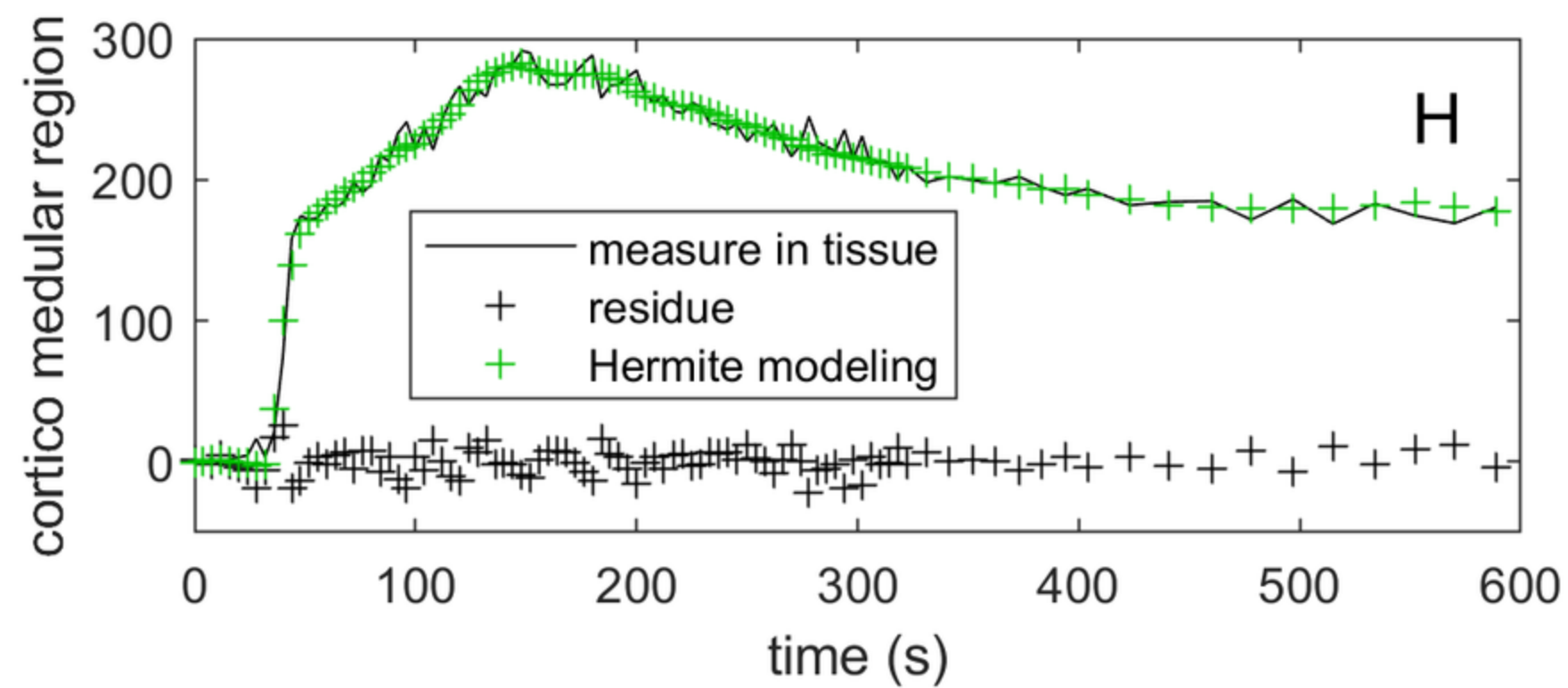
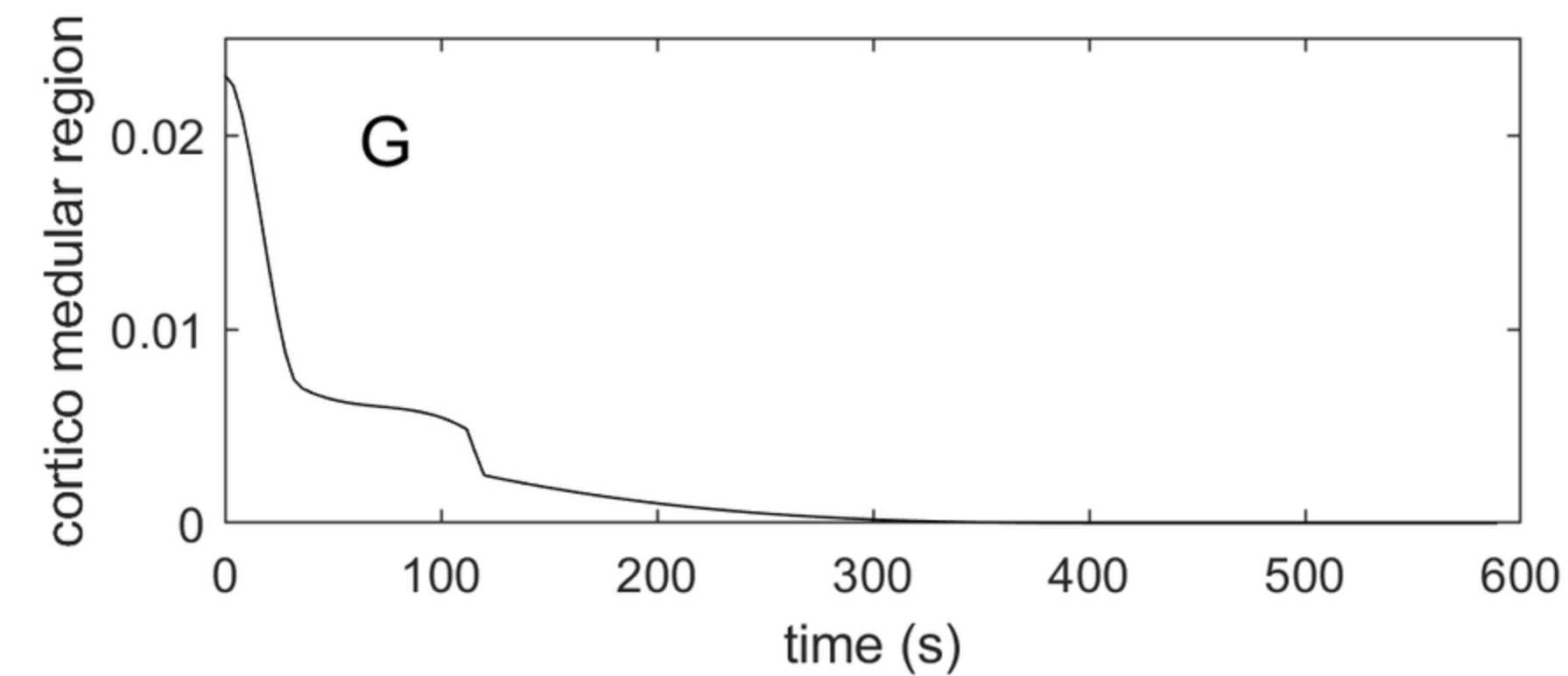
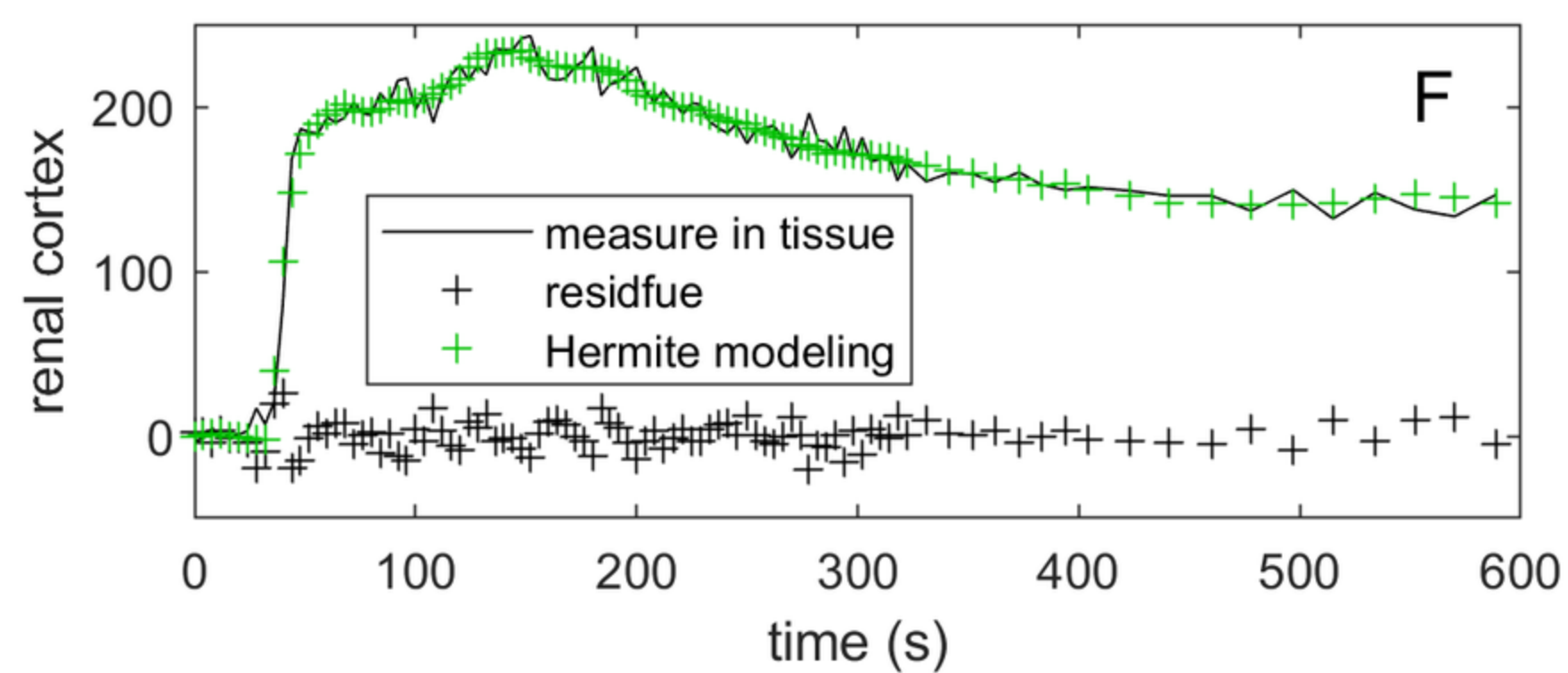
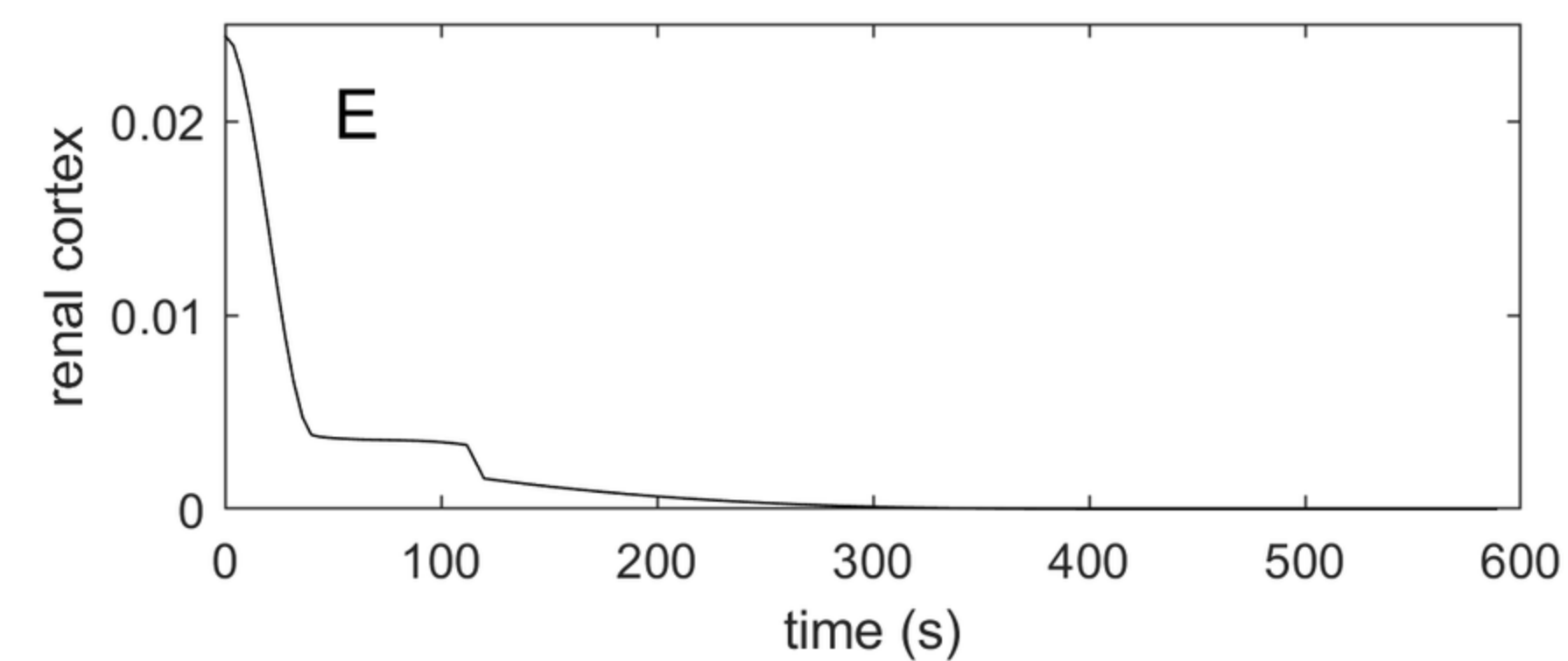
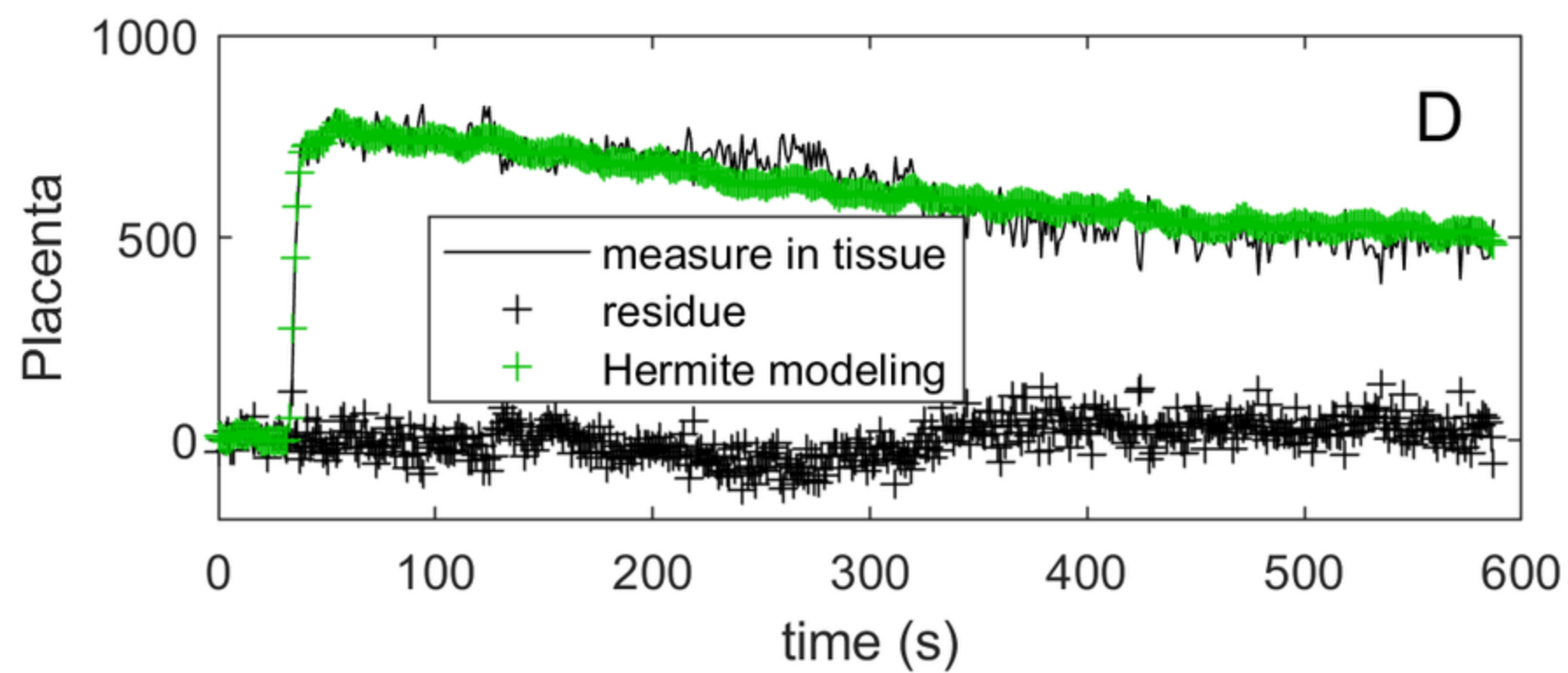
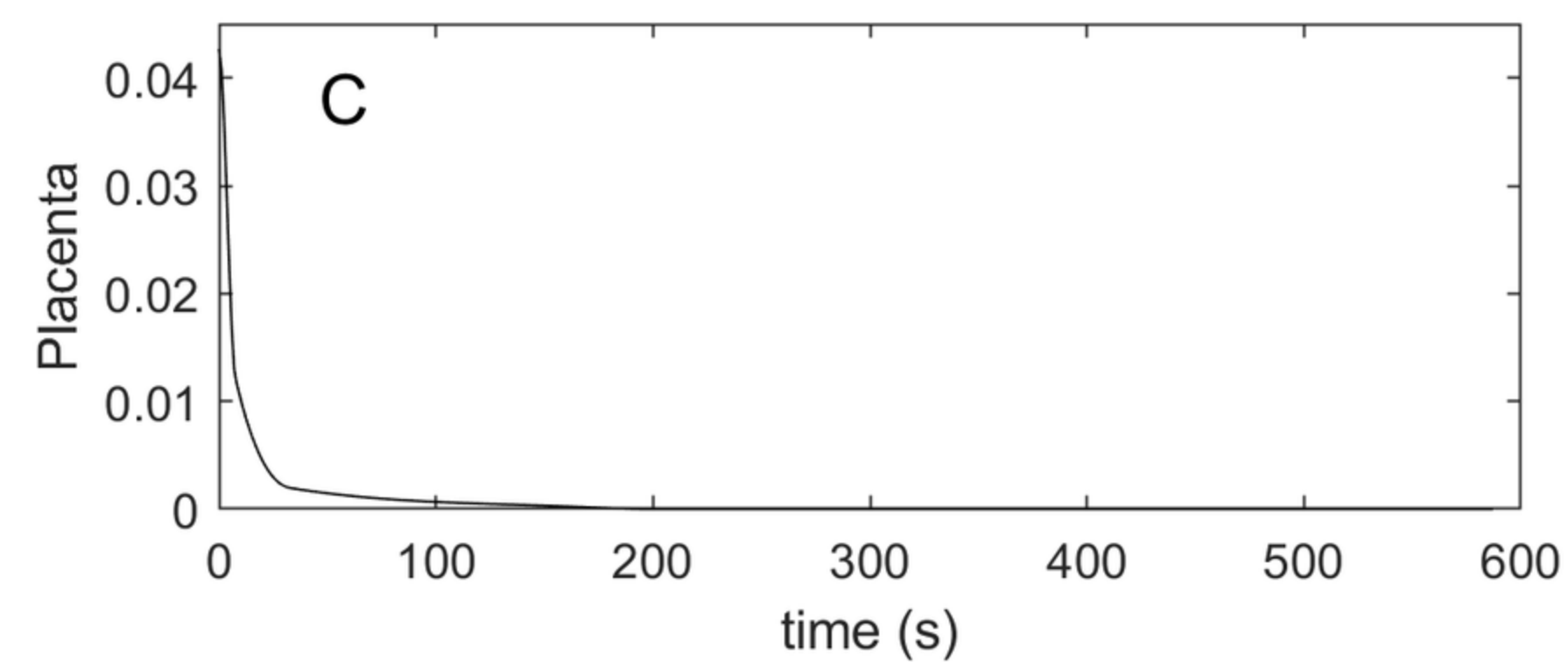
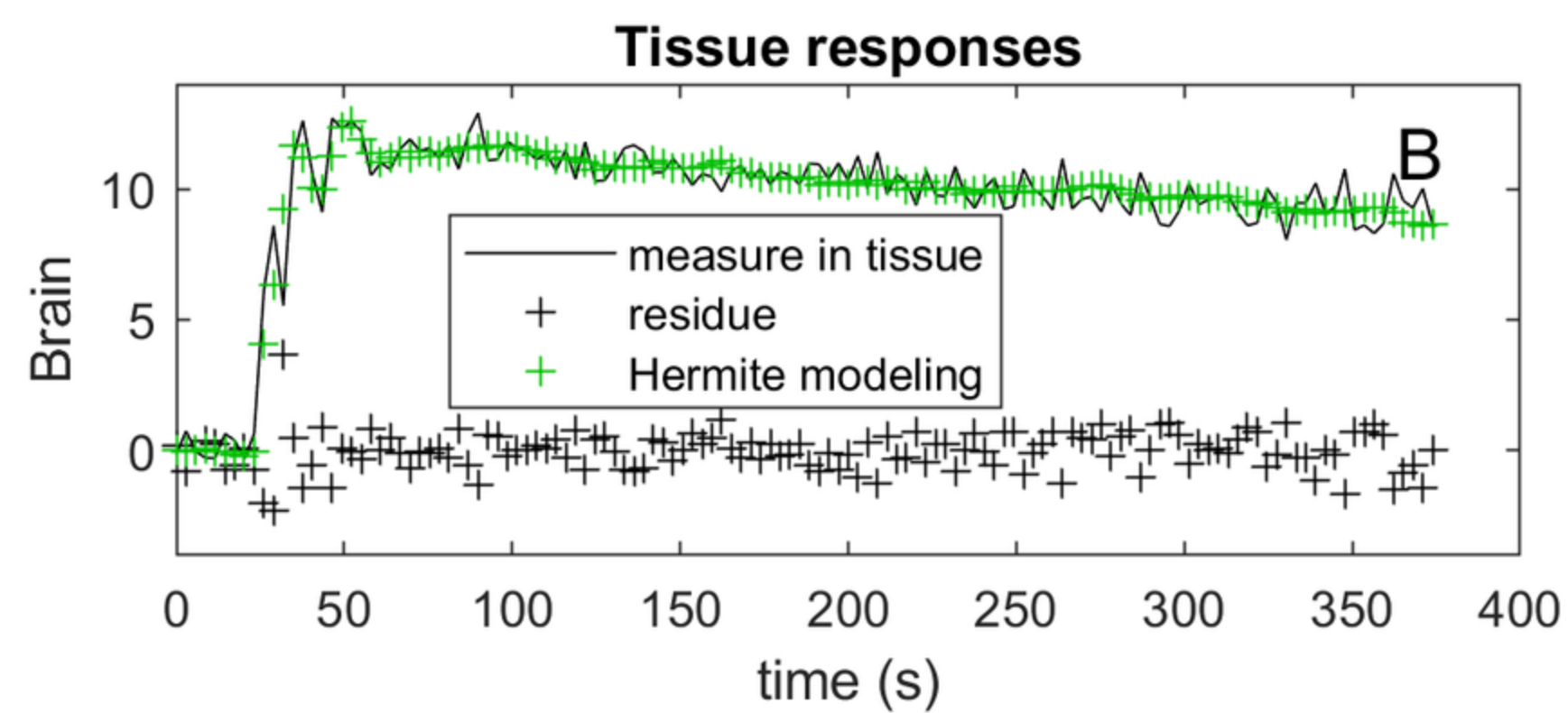
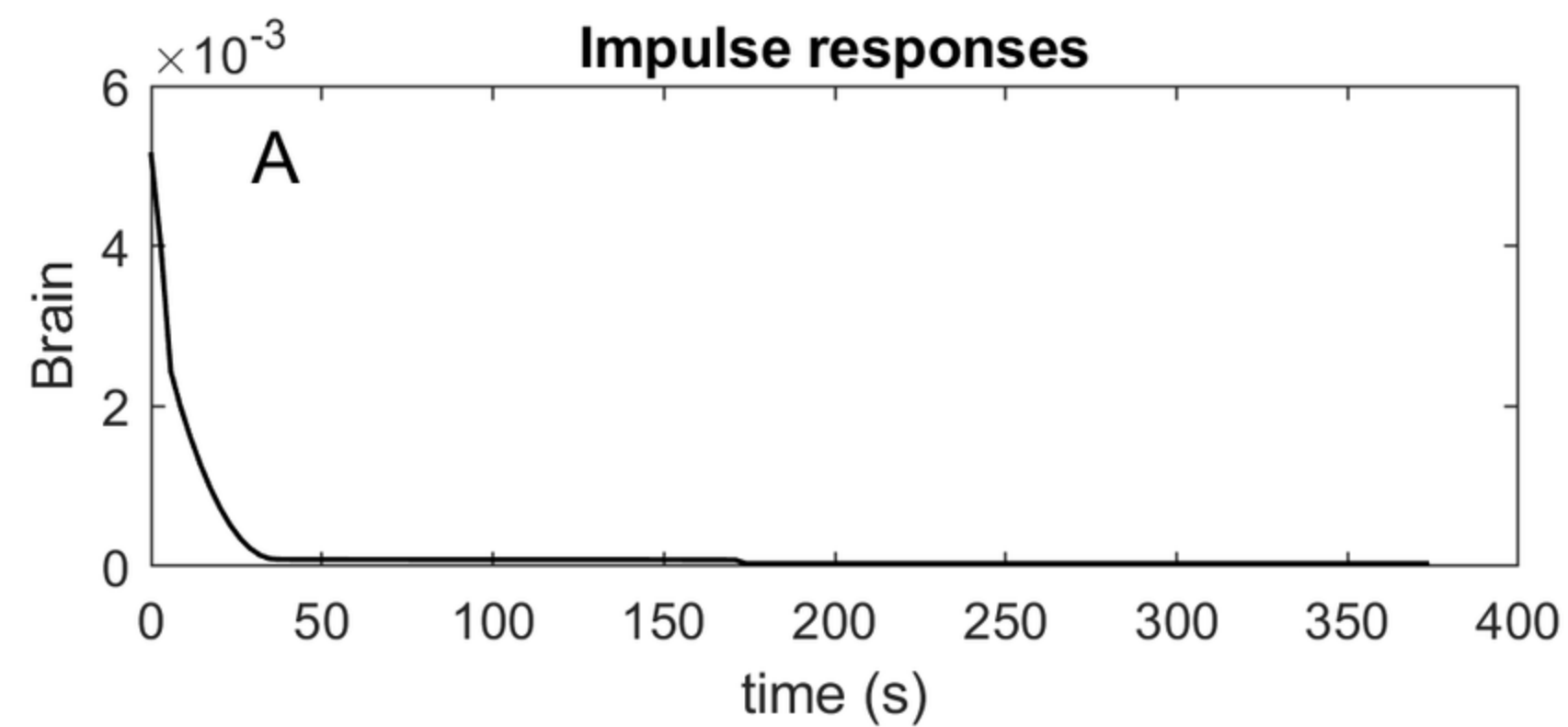
TIR_a

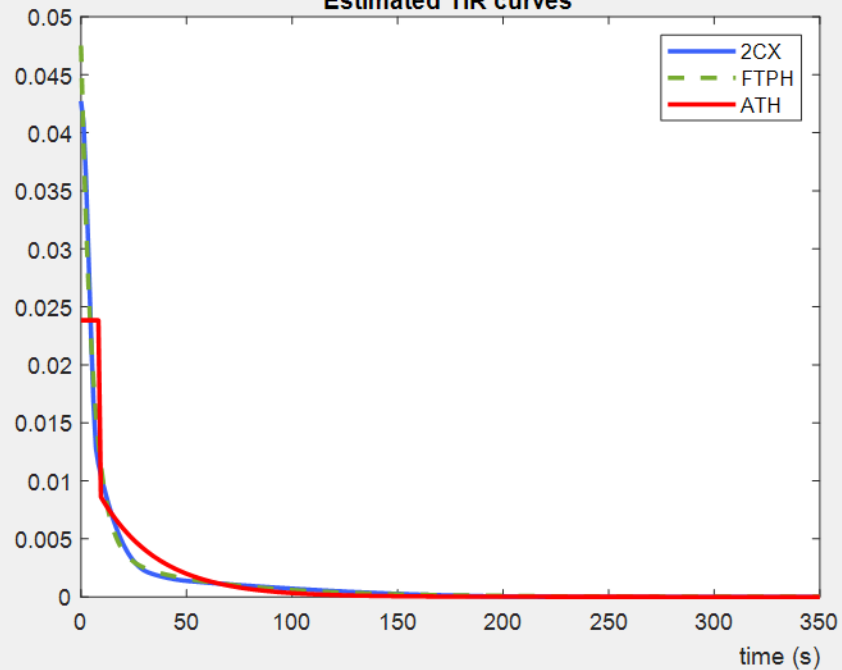
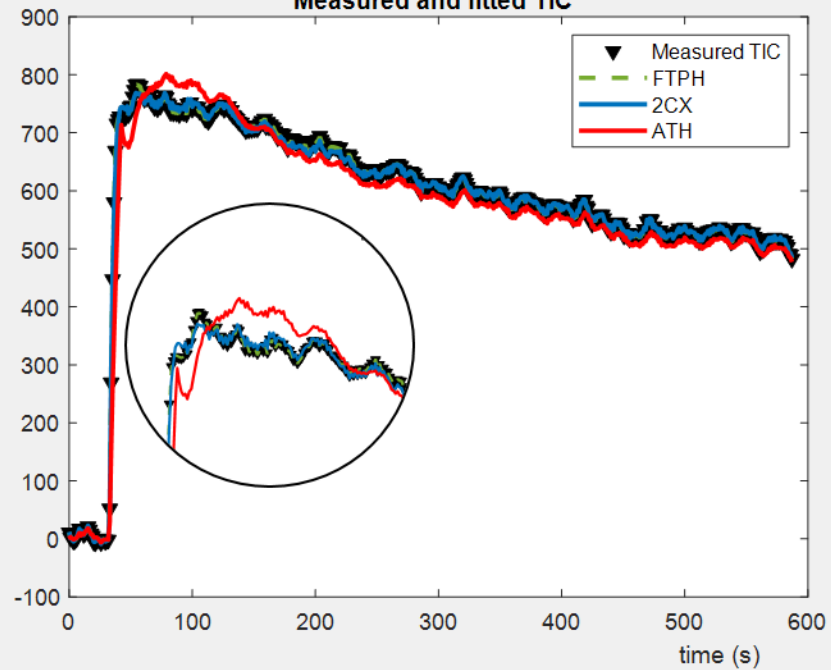
(n = 5)









Estimated TIR curves**Measured and fitted TIC**

Tissue	TR (ms)	TE (ms)	Flip Angle	Duration	Time points	Sequen- ce
Kidney (Human)	2.1	0.9	15°	99s	589	3D
Brain (Human)	4	2.3	8°	373s	130	3D
Placenta (Rat)	11.4	1.0	90°	587s	500	2D

Table 1. Parameters of the MRI sequences

	Hermite model assessments			
	Without noise		SNR = 20	
	Sensibility	Specificity	Sensibility	Specificity
ATH	91 (\pm 9) %	98 (\pm 5) %	86 (\pm 12) %	83 (\pm 13) %
2CX	97 (\pm 5) %	93 (\pm 10) %	80 (\pm 11) %	86 (\pm 12) %
	B-spline model assessments			
	Without noise		SNR = 20	
	Sensibility	Specificity	Sensibility	Specificity
ATH	56 (\pm 16) %	99 (\pm 2) %	46 (\pm 16) %	94 (\pm 5) %
2CX	98 (\pm 5) %	70 (\pm 17) %	85 (\pm 8) %	67 (\pm 5) %

Table 2. Efficiency of the identification of pharmacokinetic hypotheses. Sensibility and specificity for Hermite and B-spline model to identify data generated with ATH and 2CX assumptions. (presented as mean values with standard deviations)

Nb ^{95%}	Hermite model		B-spline model	
	Noise-free	SNR = 20	Noise-free	SNR = 20
ATH	3.8 (± 2.17)	8.6 (± 9.32)	>16 (± 6.6)	>16 (± 0)
2CX	2.4 (± 0.5)	8.2 (± 9.55)	4.2 (± 4.9)	5.4 (± 4.3)

Table 3. Mean exams number to identify the pharmacokinetic hypothesis. Number of measures required to identify the initial pattern (2CX or ATH assumptions) with 95% of confidence, with Hermite and B-spline modeling.

E	Hermite model	
	Without noise	SNR = 20
ATH	3.35 (\pm 2.9) %	8.33 (\pm 3.9) %
2CX	2.52 (\pm 0.9) %	6.89 (\pm 2.4) %
E	B-spline model	
	Without noise	SNR = 20
ATH	15.87 (\pm 6.09) %	44.89 (\pm 83.6) %
2CX	1.16 (\pm 1.1) %	24.94 (\pm 74.4) %

Table4. Estimation error of the TIR. Modeling errors (E in %) between initial impulse responses generated with ATH and 2CX models and Hermite and B-spline estimations, for noisy (SNR = 20) and non-noisy data. Values: means with standard deviation